Cancer Microenvironment (2017) 10:57–68
DOI 10.1007/s12307-017-0197-6

ORIGINAL ARTICLE

Expression Profiling of the MAP Kinase Phosphatase Family Reveals a Role for *DUSP1* in the Glioblastoma Stem Cell Niche

Bradley N. Mills[1,2] · **George P. Albert**[2] · **Marc W. Halterman**[2,3,4]

Received: 30 April 2017 / Accepted: 9 August 2017 / Published online: 18 August 2017

Abstract The dual specificity phosphatases (DUSPs) constitute a family of stress-induced enzymes that provide feedback inhibition on mitogen-activated protein kinases (MAPKs) critical in key aspects of oncogenic signaling. While described in other tumor types, the landscape of DUSP mRNA expression in glioblastoma (GB) remains largely unexplored. Interrogation of the REpository for Molecular BRAin Neoplasia DaTa (REMBRANDT) revealed induction (*DUSP4, DUSP6*), repression (*DUSP2, DUSP7–9*), or mixed (*DUSP1, DUSP5, DUSP10, DUSP15*) *DUSP* transcription of select DUSPs in bulk tumor specimens. To resolve features specific to the tumor microenvironment, we searched the Ivy Glioblastoma Atlas Project (Ivy GAP) repository, which highlight *DUSP1*, *DUSP5*, and *DUSP6* as the predominant family members induced within pseudopalisading and perinecrotic regions. The inducibility of *DUSP1* in response to hypoxia, dexamethasone, or the chemotherapeutic agent camptothecin was confirmed in GB cell lines and tumor-derived stem cells (TSCs). Moreover, we show that loss of *DUSP1* expression is a characteristic of TSCs and correlates with expression of tumor stem cell markers *in situ* (ABCG2, PROM1, L1CAM, NANOG, SOX2). This work reveals a dynamic pattern of DUSP expression within the tumor microenvironment that reflects the cumulative effects of factors including regional ischemia, chemotherapeutic exposure among others. Moreover, our observation regarding *DUSP1* dysregulation within the stem cell niche argue for its importance in the survival and proliferation of this therapeutically resistant population.

Keywords DUSP1 · Glioblastoma multiforme · Tumor stem cell · Dexamethasone · Camptothecin · Mitogen-activated protein kinases · Hypoxia · Temozolomide

Abbreviations

DUSP1	Dual specificity phosphatase 1
GB	Glioblastoma
TSC	Tumor stem cell
DEX	Dexamethasone
CPT	Camptothecin
LE	Leading edge
CT	Bulk cellular tumor
CTpan	Cellular tumor pseudopalisading around necrosis
CTpnz	Cellular tumor perinecrotic zone

Introduction

Features of microvascular proliferation, cellular heterogeneity, bilateral invasion, and extensive necrosis define glioblastoma (GB) tumors. The accumulation of genomic mutations induce metabolic reprogramming, cellular proliferation, and enhanced survival culminating in the classical histological

Electronic supplementary material The online version of this article (doi:10.1007/s12307-017-0197-6) contains supplementary material, which is available to authorized users.

✉ Marc W. Halterman
Marc_Halterman@urmc.rochester.edu

[1] Department of Pathology and Laboratory Medicine, University of Rochester Medical Center, Rochester, NY 14642, USA

[2] Center for Neurotherapeutics Discovery, University of Rochester Medical Center, 601 Elmwood Avenue, Box 645, Rochester, NY 14642, USA

[3] Department of Neurology, University of Rochester Medical Center, Rochester, NY 14642, USA

[4] Department of Neuroscience, University of Rochester Medical Center, Rochester, NY 14642, USA

features characteristic of grade IV tumors [1, 2]. These phenotypes emerge via subsequent cycles of tumor outgrowth and secondary ischemia-induced necrosis creating marked regional heterogeneity across the tissue specimen. Specific tumor sub-regions include the leading edge consisting of the infiltrating, the bulk cellular tumor, and deeper regions characterized by neovascularization, pseudopalisading, and necrosis driven by the imbalance between metabolic supply and demand [3]. In addition to producing this regional heterogeneity within the tumor mass, intratumoral ischemia also plays a key role in the pathogenesis of glioblastoma, notably through the proliferation and self-renewal of tumor stem cells (TSCs). Defined by double labeling immunofluorescence studies of tumor stem cell markers within GB tissue specimens [4], the milieu within the perivascular and perinecrotic regions promote maintenance of TSC stem cell properties including their high rates of proliferation and chemotherapeutic resistance [5].

Mutations affecting tumor suppressor genes including *TP53* and *RB1* in tandem along with gain of function mutations in the tyrosine kinase receptor *EGFR*, among others produce synergistic oncogenic effects in glioblastoma [6]. These changes have important effects on the mitogen-activated protein kinase cascade comprised of extracellular signal-regulated kinase, c-Jun N-terminal kinase, and p38 kinase [6]. ERK, JNK, and p38 respond to a multitude of stimuli with their activation having classically been associated with a variety of cellular processes including proliferation, apoptosis, and differentiation [7, 8]. And although MAPK signaling is an attractive therapeutic target, the selective drugging of various effectors with small molecule kinase inhibitors in recurrent GB has yielded unimpressive results in the clinic [9]. Thus, identification of alternate pathways capable of attenuating MAPK signaling tone in glial tumors may have therapeutic benefit.

Under homeostatic conditions, growth factor signaling mediated by MAPKs is held in check by a family of mitogen-activated protein kinase dual-specificity phosphatases (MKP/DUSPs) that exhibit context-dependent feedback. To date, studies investigating DUSP family expression in various tumors have revealed marked diversity [8]. In the case of GBP, studies of *DUSP1* and *DUSP6* regulation argue for upregulation relative to normal tissue [10, 11]. And while somatic mutations of DUSP family members have not been reported in GB, studies have identified *DUSP4* downregulation via mechanisms involving promoter hypermethylation [12]. Early studies also indicate that *DUSPs* respond dynamically to a variety of stimuli present in the tumor microenvironment including mitogenic stimulation [13], differentiation [14], ischemia [15], and exposure to corticosteroids and chemotherapeutics [16].

Given the importance of MKP/DUSP negative feedback on mitogenic signaling and the body of evidence linking their dysregulation in other cancer models, we asked whether changes in *DUSP* transcription contribute to unrestrained proliferation and therapeutic resistance observed in GB tumors. Our results indicate that the family of DUSPs exhibit marked heterogeneity across the tumor microenvironment. Further analysis of these trends suggested that *DUSP1* dysregulation may play a particularly important role in regulating the tumor stem cell compartment in glial tumors.

Materials and Methods

REMBRANDT Microarray Analysis The REpository for Molecular BRAin Neoplasia DaTa (REMBRANDT) database contains 228 pathologically confirmed cases of mixed primary and secondary GB including four, tumor re-resections that were subjected to expression profiling using the Affymetrix HG_U133 gene chips with the highest geometric mean intensity [17]. Sample data values were distributed as fold changes from the geometric mean of normal brain tissue obtained from patients undergoing surgical resection for medically refractory temporal lobe epilepsy (TLE).

Cerebral Cortex RNA-Seq Analysis *DUSP* expression profiles were analyzed using the Barres RNA-Seq transcriptome generated from eight cell types present in the mouse cortex (web.stanford.edu/group/barres_lab/brain_rnaseq). Single cell suspensions were generated from the cortices of postnatal mice and purified by FACS sorting for cell-specific markers as described by Zhang et al. prior to RNA-seq analysis [18]. Although data were obtained for eight different cellular populations, we focused our analyses on oligodendrocyte progenitors (OPCs), astrocytes, microglia, and neurons. FPKM values were plotted for each dataset.

Ivy Glioblastoma Atlas Project RNA-Seq Analyses RNA-seq datasets of total cell and TSC-only human tissue samples were downloaded from the Ivy Glioblastoma Atlas Project (Ivy GAP) website (http://glioblastoma.alleninstitute.org/rnaseq) [19]. Each dataset contained samples that were microdissected based on sub-regional localization prior to transcriptional analyses. Briefly, 122 RNA samples were curated from 10 grade IV GB tumors that were microdissected into five structural groups using ISH panels to identify regionally enriched genesets. For TSC sample isolation, a panel of seventeen GB TSC markers was used by Ivy GAP to identify and isolate GB TSC clusters within GB biopsy specimens that localized with micro environmental region markers.

The Cancer Genome Atlas Analyses Gene expression datasets from grade IV GB samples analyzed by Affymetrix HT_HG-U133A microarray gene chips were curated from the Cancer Genome Atlas (TCGA) data portal [20]. R-values

were computed between datasets not assumed to be sampled from Gaussian distributions using nonparametric Spearman correlation analysis. For heat map images, values for each gene target were first normalized to the maximum expression value within that geneset. Expression values were next sorted from max to min DUSP1 expression for each sample, before stratification into ten sample bins that were displayed as an average gene expression.

Transcriptional Analyses of Primary Glioblastoma Tumors Clinical specimens used in this study were provided by the Neurosurgical Brain Tissue Bank of the University of Rochester under protocol #00049707 approved by the University of Rochester Research Subjects Review Board. Grade IV GB and epileptic control tissues were stored at −80°C prior to total RNA isolation. To harvest RNA, Buffer RLT and homogenizer beads were added to samples prior to agitation for three minutes and transfered to QIAshredder spin columns (Qiagen, Valencia, CA, USA). Cells were harvested for total mRNA using the RNeasy kit (Qiagen, Valencia, CA, USA) and cDNA was reverse transcribed using the iScript cDNA Synthesis kit (Bio-Rad, Hercules, CA, USA) for Taqman probe-based quantitative PCR reactions of human *DUSP1* (FAM-MGB, Hs00610256_g1), *DUSP2* (FAM-MGB, Hs00358879_m1), *DUSP7* (FAM-MGB, Hs00997002_m1), and *DUSP8* (FAM-MGB, Hs01014943_m1) (Life Technologies (Grand Island, NY, USA). *18SRRNA* (VIC-MGB, Hs03003631_g1) was used as an internal reference gene for standardization in multiplex reactions. $\Delta\Delta C_T$ analysis was performed for relative quantification of target gene regulation relative to control samples.

Cell Culture U251 and U343 tumor cells (obtained from Dr. Carson-Walter, University of Rochester, Rochester, NY) were maintained in DMEM, high glucose with L-glutamine, sodium pyruvate, and 1× penicillin-streptomycin (Life Technologies, Grand Island, NY, USA), supplemented with 10% heat-inactivated fetal bovine serum (Innovative Research, Novi, MI, USA). GB TSCs obtained from Dr. Angelo Vescovi (IRCSS Casa Sollievo della Sofferenza, Opera di San Pio da Pietrelcina, viale dei Cappuccini, 1, 71,013 S. Giovanni Rotondo, Italy) [21] were maintained in DMEM/F12 with L-glutamine (Corning Life Sciences, Tewksbury, MA, USA) and 1× penicillin-streptomycin, supplemented with B-27 minus vitamin A (Thermo Fisher Scientific, Waltham, MA, USA), 20 ng/mL EGF, and 20 ng/mL bFGF (Peprotech, Rocky Hill, NJ, USA). Differentiation of GB TSCs was performed by plating cells on 60-mm laminin-coated plates (Sigma-Aldrich, St. Louis, MO, USA) in DMEM/F12 with L-glutamine and 1× penicillin-streptomycin, supplemented with 5% fetal bovine serum for a minimum of 3 days prior to harvest. In all conditions, cells were passed at 37°C under humidified, (21% O_2) conditions supplemented with 5% CO_2 (BINDER, Bohemia, NY, USA).

Flow Cytometry GB TSCs were plated at 500 cells/mm^2 72 h prior to harvest. Upon harvest, cells were fixed in 10% paraformaldehyde for 25 min and permeabilized in 0.5% Triton X-100 for 15 min before incubating with primary antisera. Staining for anti-SOX2-V450, anti-GLAST1-APC, and anti-NEUROD1-PE (BD Biosciences, San Jose, CA), was carried out for 30 min at 4°C in the dark. Forward scatter, side scatter, Violet C (V450), Red C (APC), and Blue E (PE) were collected on a 3-laser, 12-color BD LSR-II platform (BD Biosciences) and FlowJo software (FLOWJO, Portland, OR) were used for analysis. Data from 10,000 cells was collected, and live cells were gated using forward and side scatter data prior to fluorescence analyses.

Hypoxia/Drug Treatments U251 cells and GB TSCs were plated at 400 and 250 cells/mm^2, respectively, and incubated overnight under normal conditions. Hypoxic incubations were carried out under 0.5% O_2 / 5% CO_2 conditions in a Binder incubator. Drug stocks were reconstituted as follows: CPT (C9911; Sigma-Aldrich), 10 mM in DMSO; DEX (D2915; Sigma-Aldrich), 0.25 mM in dd$H_2$0; TMZ (sc-203,292; Santa Cruz Biotechnology), 10 mM in ddH_2O; and TOPO (sc-204,919; Santa Cruz Biotechnology), 0.3 mM in ddH_2O and treatments were administered for 24 h prior to cell harvest.

Statistical Analyses All statistical comparisons were performed using the GraphPad Prism application. REMBRANDT and gene expression data from the URMC brain bank tumor specimens were analyzed using column statistics to calculate medians, standard deviations, and interquartile ranges. R-values were computed between datasets not assumed to be sampled from Gaussian distributions using nonparametric Spearman correlation analysis. GB microenvironment regional DUSP expression identified in the Ivy Allen Brain Dataset analyses, the primary tumor analyses, and *in vitro* analyses of *DUSP1* regulation in both TSCs and established GB tumor lines were expressed as the mean ± standard deviation and were tested by one-way ANOVA using the Bonferroni test for multiple comparisons. Results with *p*-values less than 0.05 were considered significant.

Results

Profiling DUSP Expression in GB Tumors To assess changes in *MKP/DUSP* expression within GB samples, we interrogated the REMBRANDT dataset plotting the expression of the ten active family members for each tumor specimen (n = 228) relative to non-tumorigenic brain tissue. Although results show significant variation in DUSP expression across

clinical subjects, we observed several key trends in both the magnitude and direction of the average response (Fig. 1). In the first group including *DUSP1* (1.41, IQR = 1.40), *DUSP5* (1.04, IQR = 0.73), *DUSP10* (0.96, IQR = 0.51), and *DUSP16* (1.04, IQR = 0.53) gene expression changes were modest, exhibiting less than a two-fold change with little directional skew. The second group of targets including *DUSP2* (0.24, IQR = 0.45), *DUSP7* (0.57, IQR = 0.60), *DUSP8* (0.33, IQR = 0.27), and *DUSP9* (0.58, IQR = 0.40) exhibited greater than two-fold reductions in gene expression with relatively few outliers. Conversely, *DUSP4* (3.22, IQR = 4.44) and *DUSP6* (2.34, IQR = 2.41) showed greater than two-fold inductions in gene expression in the majority of samples. Given their prominence in the literature and distinct patterns of expression, we performed qPCR analysis for *DUSP1* and *DUSP2* from a cohort of grade IV primary GB samples deposited at the University of Rochester Brain Bank to corroborate these findings. Results demonstrate that, on average, *DUSP1* levels were unchanged relative to epileptic controls (1.0 ± 0.44 vs. 1.65 ± 2.34; $p = 0.822$) while *DUSP2* (1.0 ± 0.43 vs. 0.33 ± 0.38; $p = 0.020$), *DUSP7* (1.0 ± 0.45 vs. 0.17 ± 0.15; $p = 0.003$), and *DUSP8* (1.0 ± 0.37 vs.

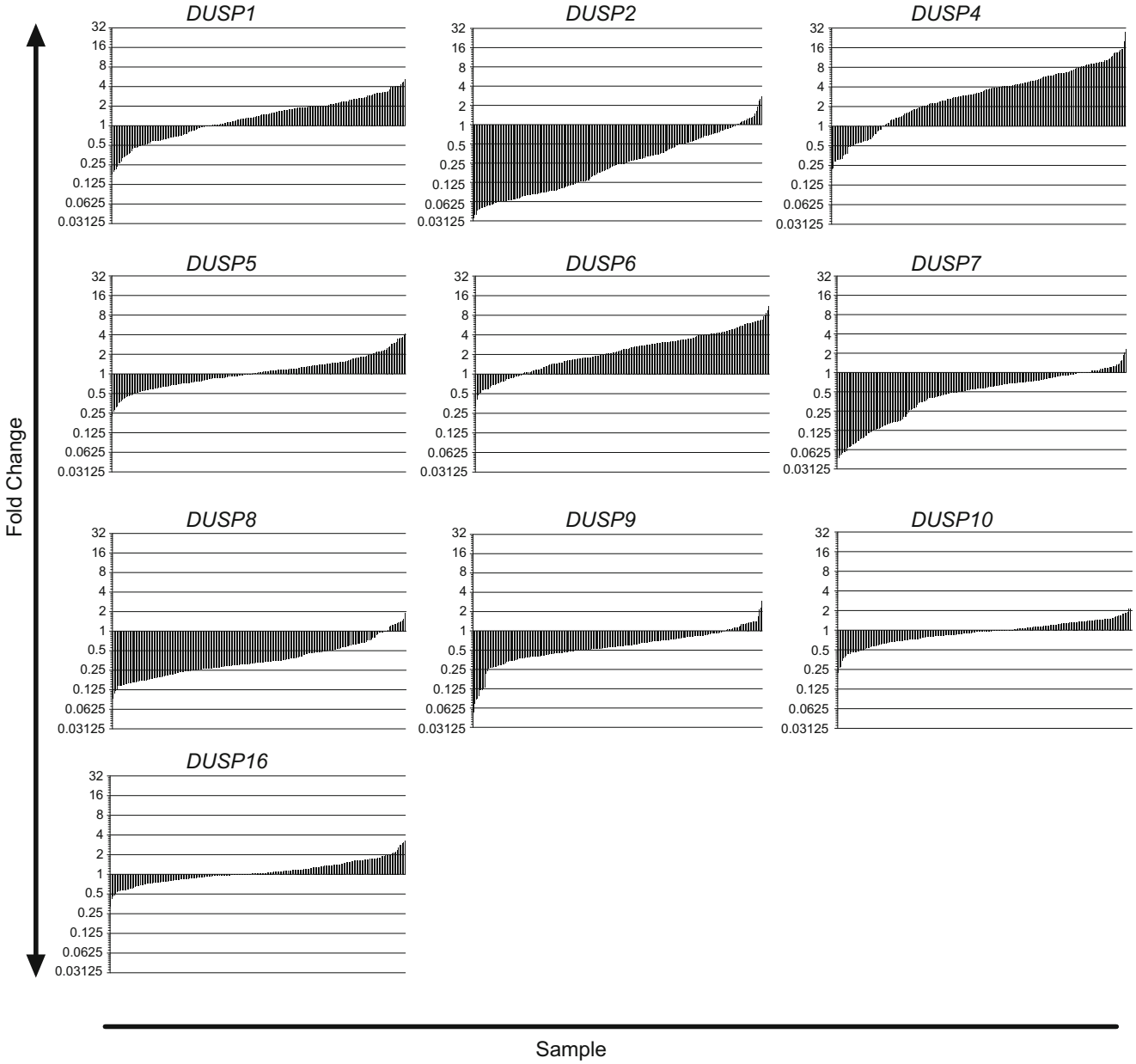

Fig. 1 Microarray profiling of *DUSPs* across mixed primary and secondary GB tumors. Histograms depicting the fold change in mRNA expression for each of the DUSP members analyzed using the REMBRANDT Microarray dataset. Gene expression levels for each GB tumor ($n = 228$) are presented as fold change relative to the average level across normal tissue controls ($n = 28$) and plotted on a log2 scale

0.33 ± 0.21; $p = 0.003$), expressions were significantly down-regulated comparable to changes observed in the REMBRANDT analysis (Fig. 2).

Effects of Tumor Cellular Composition and Microenvironment on *DUSP* Expression in GB We next asked whether the transition away from the transcriptional composition of normal brain parenchyma, towards a glial-type phenotype characteristic of GBM, might explain the shifting expression of DUSP family members observed in the REMBRANDT dataset. To test this hypothesis, we first compared *Dusp* expression in purified mouse glia against levels in neurons, oligodendroglia, among other cell types isolated by immunopanning from the cerebral cortex with the Barres RNA-Seq database [18]. Results demonstrate considerable differences in *Dusp* expression across the four lineages analyzed (Fig. 3a). Overall, *Dusp1 and Dusp6 were* the most highly expressed dual specificity phosphatase across all cell types. Other trends were noted, including expression peaks in microglia (*Dusp2*, *Dusp6),* astrocytes *(Dusp1, Dusp6),* and neurons *(Dusp1*, *Dusp4*, *Dusp8*). To corroborate these results, we performed a secondary RNA-seq analysis using the Ivy Glioblastoma Atlas database (IvyGAP) [19]. The Ivy dataset is comprised of 122 RNA samples from ten GB tumors that were laser micro-dissected into five structural groups using ISH panels to identify regionally enriched genesets. The leading edge (LE) on the outer rim of the tumor contains the highest ratio (50:1) of normal to cancerous tissue. Comparable to our prior analyses, we found that *DUSP1* expression (39.0 ± 49.8) was significantly higher ($p < 0.0001$) than all other *DUSP* members except *DUSP6* (32.1 ± 17.0) (Fig. 3b).

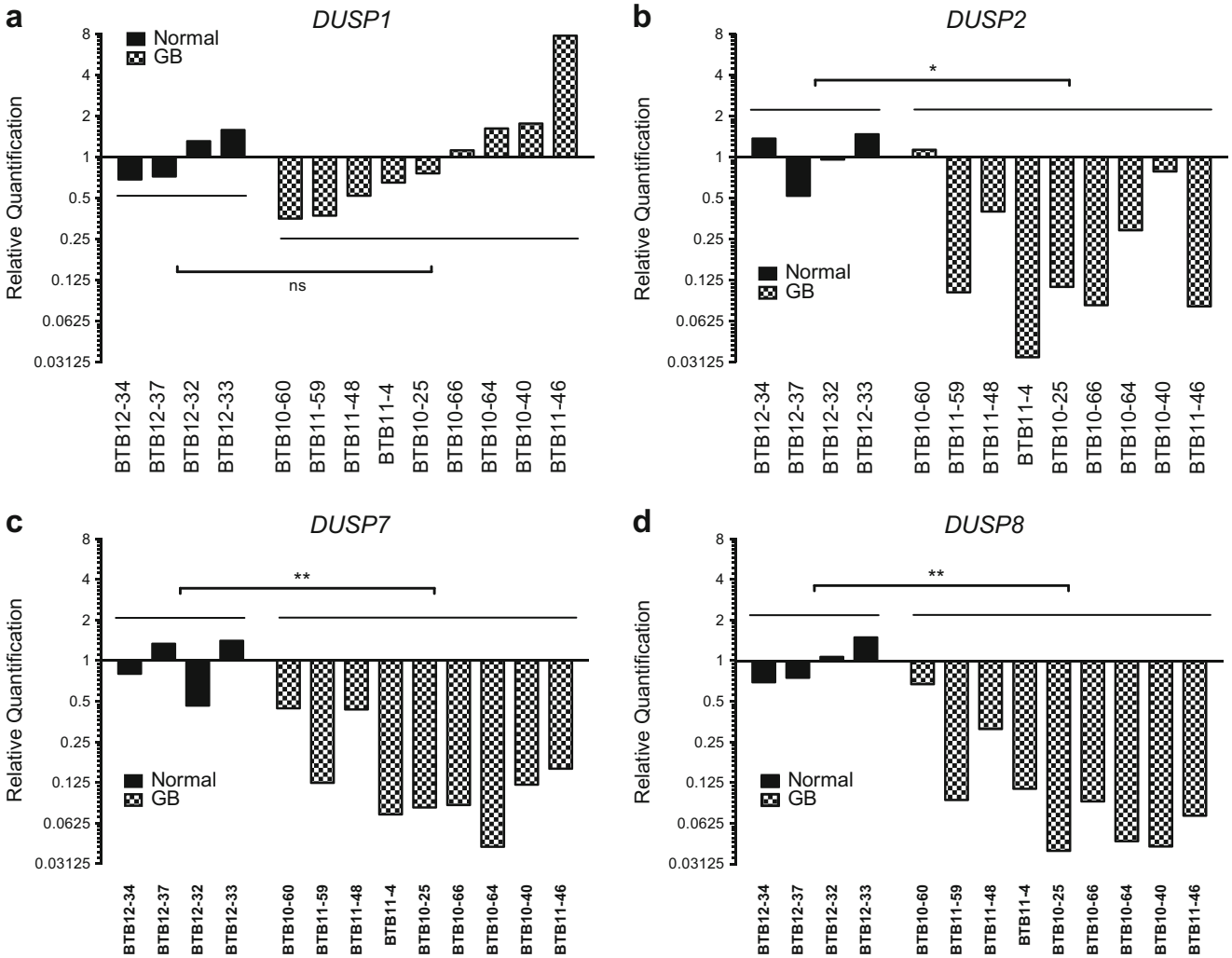

Fig. 2 Quantitative PCR analysis of *DUSP* expressions in epileptic control and grade IV GB tumors. Quantitative PCR analysis of *DUSP1, DUSP2, DUSP7,* and *DUSP8* expression in human grade IV GB tissue samples (GB, $n = 9$) and temporal lobe epileptic controls (normal, $n = 4$) maintained by the University of Rochester Brain Tissue Bank. Fold-induction data are presented relative to the average expression of the comparator gene within epileptic controls and presented using a log2 scale. Statistical significance was measured across groups by one-way ANOVA (ns = not significant, * = $p < 0.05$, ** = $p < 0.01$)

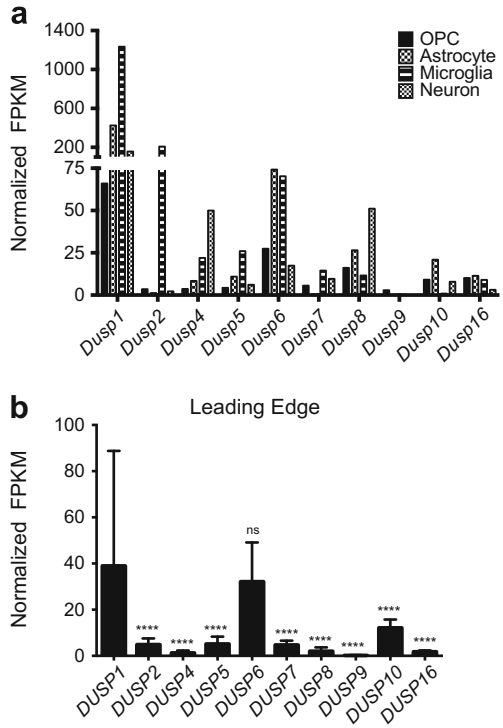

Fig. 3 Cell type and region specific profile of *DUSP* expression. **a** RNA-Seq expression levels of the *Dusp* family obtained from the Barres online dataset presented as normalized fragments per kilobase of transcript per million mapped reads (FPKM) across various cell types. RNA-Seq data were originally generated from purified oligodendrocyte precursor cell (OPC), astrocyte, microglia, and neuronal populations isolated from mouse P7 cortices by immunopanning (n = 19) as described [18]. **b** Analysis of *DUSP* expression within the "normal" leading edge (LE) of human GB tumors. RNA-Seq data from the Ivy GAP database are presented. LE regions of GB biopsy samples (50:1 normal:tumor cells) were identified using ISH panels and microdissected by the Ivy GAP consortium prior to RNA-Seq analysis. The data in (b) are presented as the average ± standard deviation, and statistical significance was determined using one-way ANOVA with Bonferroni correction for multiple comparisons (*DUSP1* vs. all datasets; ns = not significant, **** = $p < 0.0001$)

Given the observed variability in expression of select DUSPs across clinical specimens, we considered whether parsing factor expression based on regional physiological changes across the tumor microenvironment might be informative. To test this, we profiled *DUSP* expression within the leading edge (LE), bulk cellular tumor (CT), pseudopalisading around necrosis (CTpan), and perinecrotic (CTpnz) zones dissected from human GB samples using laser capture microdissection followed by RNA-seq as described [19]. Using LE regional expression as the control reference, we found that the general trends in expression were consistent with the REMBRANDT analyses. Relative to LE controls, FPKM values for *DUSP2* (LE: 4.9 ± 2.7; CT: 0.2 ± 0.3; CTpan: 0.4 ± 0.5; CTpnz: 0.8 ± 1.4; $p < 0.0001$), *DUSP7* (LE: 4.7 ± 1.9; CT: 2.1 ± 1.6; CTpan: 1.4 ± 0.8; CTpnz: 2.1 ± 1.3; $p < 0.0001$), and *DUSP8* (LE: 2.0 ± 1.6; CT: 0.3 ± 0.2; CTpan: 0.3 ± 0.2; CTpnz: 0.4 ± 0.2; $p < 0.0001$) were downregulated in all tumor regions. Conversely, FPKM values for *DUSP4* (LE: 1.3 ± 1.1; CT: 2.4 ± 2.1, ns; CTpan: 5.4 ± 4.9, $p < 0.001$; CTpnz: 3.6 ± 3.0, ns), *DUSP6* (LE: 32.1 ± 17.0; CT: 109.6 ± 114.0, $p < 0.01$; CTpan: 94.5 ± 61.3, $p < 0.05$; CTpnz: 99.8 ± 55.5, $p < 0.05$), *DUSP10* (LE: 12.1 ± 3.6; CT: 15.4 ± 10.3, ns; CTpan: 27.5 ± 20.6, $p < 0.001$; CTpnz: 18.6 ± 7.4, ns), and *DUSP16* (LE: 1.8 ± 0.6; CT: 2.6 ± 1.0, $p < 0.05$; CTpan: 3.2 ± 1.1, $p < 0.01$; CTpnz: 2.8 ± 1.1, $p < 0.0001$) increased. Notably, the expression of both *DUSP1* (LE: 40.0 ± 49.8; CT: 18.1 ± 7.9, ns; CTpan: 62.9 ± 26.9, ns; CTpnz: 119.7 ± 114.1, $p < 0.001$; CT vs CTpan: ns; CT vs CTpnz: $p < 0.0001$) and *DUSP5* (LE: 5.1 ± 3.2; CT: 3.4 ± 2.4, ns; CTpan: 8.0 ± 3.5, ns; CTpnz: 10.3 ± 8.2, $p < 0.01$; CT vs CTpan: $p < 0.01$; CT vs CTpnz: $p < 0.0001$) were initially reduced in CT regions with subsequent induction in regions of tumor necrosis (CTpan and CTpnz; Fig. 4).

Oxygen-Dependent Expression of *DUSP1* in GB The observed relationship between *DUSP1* expression and tumor sub-region argued strongly that ischemia and among other physiological perturbations were driving *DUSP* responses *in situ* [15]. To compare *DUSP1* regulation against other oxygen-dependent genes, we identified a set of transcriptional targets regulated by the hypoxia-inducible factor 1 alpha (*HIF1A*). Non-parametric Spearman correlation analyses on microarray data from the Cancer Genome Atlas (TCGA) database (n = 547) [20] revealed that *DUSP1* expression matched that of other hypoxia-inducible genes in GB clinical specimens (Fig. 5a). The *HIF1A* targets analyzed included *BNIP3* (r = 0.11, p = 0.009), *MET* (r = 0.34, $p < 0.0001$), *PDK1* (r = 0.18, $p < 0.0001$), *SLC2A1* (r = 0.21, $p < 0.0001$), and *VEGFA* (r = 0.25, $p < 0.0001$). To confirm hypoxic regulation *in vitro*, we performed qPCR analyses on tumor-derived cell lines and patient tumor-derived stem cells (TSCs) (Fig. 5b). Results demonstrate that hypoxia stimulated *DUSP1* expression in both the U251 (1.00 [+1.22, −0.55] vs. 8.92 [+2.37, −1.87], $p < 0.01$) and U343 (1.00 [+0.10, −0.09] vs. 5.55 [+5.10, −2.66], $p < 0.05$) cell lines. Interestingly, while hypoxia-induced *DUSP1* transcriptional induction was present in undifferentiated TSCs (TSC: 2.45 [+0.62, −0.49], $p < 0.001$), the effect was increased five-fold upon TSC differentiation (10.54 [+0.82, −0.6], $p < 0.0001$).

Chemotherapeutic Induction of *DUSP1* in GB Cells Given the marked variability of *DUSP1* expression observed across tumor specimens, we next asked to what extent chemotherapeutic exposure might be involved. To test this, we performed qRT-PCR for DUSP1 in both tumor-derived cell lines and TSCs treated with the first-line agents dexamethasone (DEX) and temozolomide (TMZ), as well as the second-line topoisomerase I inhibitor camptothecin (CPT), and its analog topotecan (TOPO) (Fig. 6a). While the steroid DEX-induced *DUSP1* expression in U251 cells relative to control (2μM:

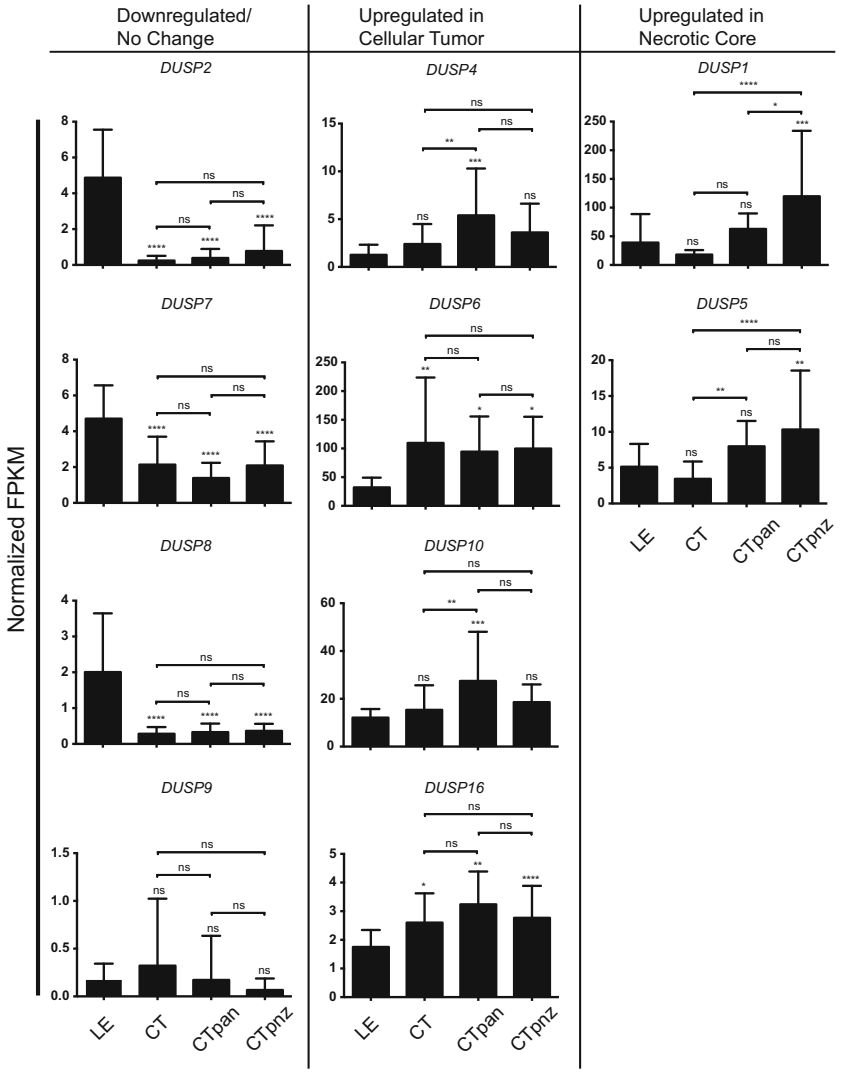

Fig. 4 Differential *DUSP* expression across the GB tumor microenvironment. The expression of *DUSP* family across discrete regions of the tumor microenvironment are shown. Data obtained from the Ivy GAP consortium are presented as normalized fragments per kilobase of transcript per million mapped reads (FPKM). Regions of GB biopsy samples including the "normal" leading edge (LE, $n = 19$), bulk cellular tumor (CT, $n = 11$), pseudopalisading cells around necrosis (CTpan, $n = 40$), and perinecrotic zone (CTpnz, $n = 26$) were identified using ISH panels prior to laser-capture microdissection. "Downregulated/No Change" and "Upregulated in Cellular Tumor" groups include DUSPs with unchanged/decreased or increased expressions in tumor structures (CT, CTpan, CTpnz) relative to "normal" LE tissues, respectively. The "Upregulated in Necrotic Core" group represents *DUSPs* with increased expression in only necrotic CTpan and CTpnz regions relative to LE. Statistical significance was determined using one-way ANOVA with Bonferroni correction to correct for multiple comparisons (ns = not significant, * = $p < 0.05$, ** = $p < 0.01$, *** = $p < 0.001$, **** = $p < 0.0001$)

4.71 [+1.24, −0.98], $p < 0.0001$), a range of TMZ dosing had no discernable effect (1.00 [+0.33, −0.25] vs. 1.19 [+0.21, −0.17], $p = 0.233$). Induction responses were observed at both doses of CPT (1μM: 15.5 [+1.06, −0.10], $p < 0.0001$). We also assessed drug effects in undifferentiated, patient-derived TSCs. Unexpectedly, neither TMZ nor DEX had an appreciable effect on mean *DUSP1* expression values relative to vehicle controls (400μM TMZ: 1.78 [+1.40, −0.78], $p = 0.419$; 10μM DEX: 1.34 [+0.27, −0.22], $p = 0.523$). Conversely, topoisomerase I inhibition remained active, inducing *DUSP1* transcription at both doses tested (20μM TOPO: 7.75 [+1.82, −1.47], $p < 0.0001$) (Fig. 6b).

***DUSP1* Expression Correlates with Markers of TSC Differentiation** Differentiation induces *DUSP1* transcription in pre-adipocytes [22], human embryoid bodies [23], and breast cancer cells [24]. To determine whether the variability in *DUSP1* expression observed in clinical GB samples may also reflect the contribution of $DUSP1^{LOW}$ stem cell populations within tumors, we evaluated the relationship between DUSP expression and that of several tumor stem cell markers reported in the TCGA database (Fig. 7a). mRNA levels of the tumor stem cell markers ATP-binding cassette subfamily G member 2 (*ABCG2*), promonin 1 (*PROM1*), L1 cell adhesion molecule (*L1CAM*), Nanog homeobox (*NANOG*), and SRY-

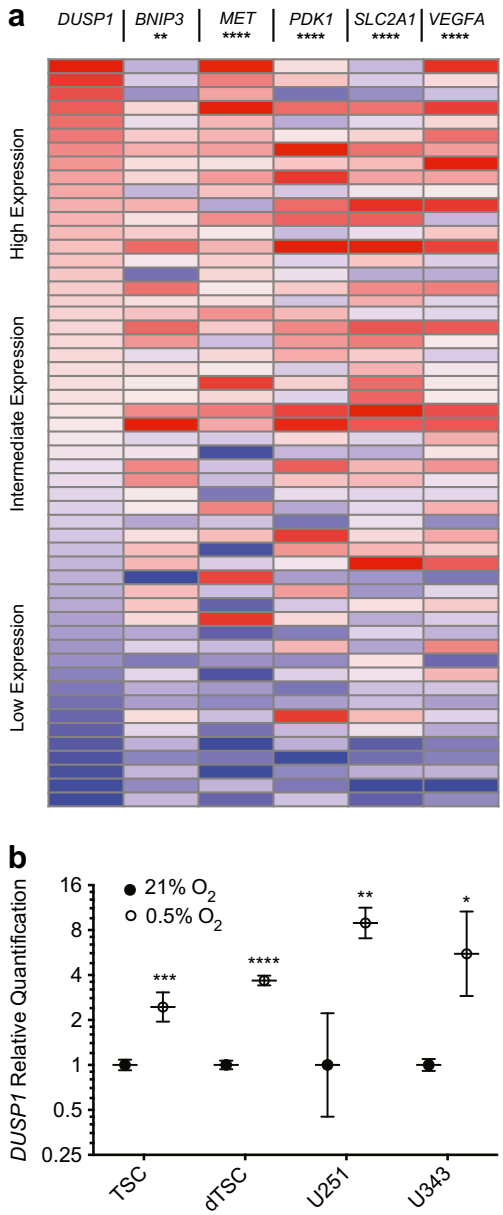

Fig. 5 Hypoxia induces *DUSP1* in cultured GB tumor cell lines. **a** Expression heat maps illustrating gene expression profiles for *DUSP1, BNIP3*, *MET*, *PDK1*, *SLC2A1*, and *VEGFA* from the TCGA GB microarray dataset ($n = 547$). For each gene, expression was normalized to the maximum expression values, sorted from max to min *DUSP1* expression, and stratified into ten sample bins that are displayed as an average gene expression heatmap. Statistical comparisons between *DUSP1* and five HIF1A transcriptional targets were performed using two-tailed, non-parametric Spearman correlation. **b** qPCR analysis of *DUSP1* expression within GB tumor stem cells, serum-differentiated tumor stem cells (dTSCs), and U251/U343 GB cell lines cultured under normoxic (21% O_2) or hypoxic (0.5% O_2, 24 h) conditions. Data are presented as quantification relative to the average of normoxic controls on a log2 scale ($n = 3$ per group). Statistical analyses were performed using one-way ANOVA. (* = $p < 0.05$, ** = $p < 0.01$, *** = $p < 0.001$, **** = $p < 0.0001$)

box 2 (*SOX2*) were extracted and plotted relative to the gradient of *DUSP1* mRNA levels across these samples [25–27].

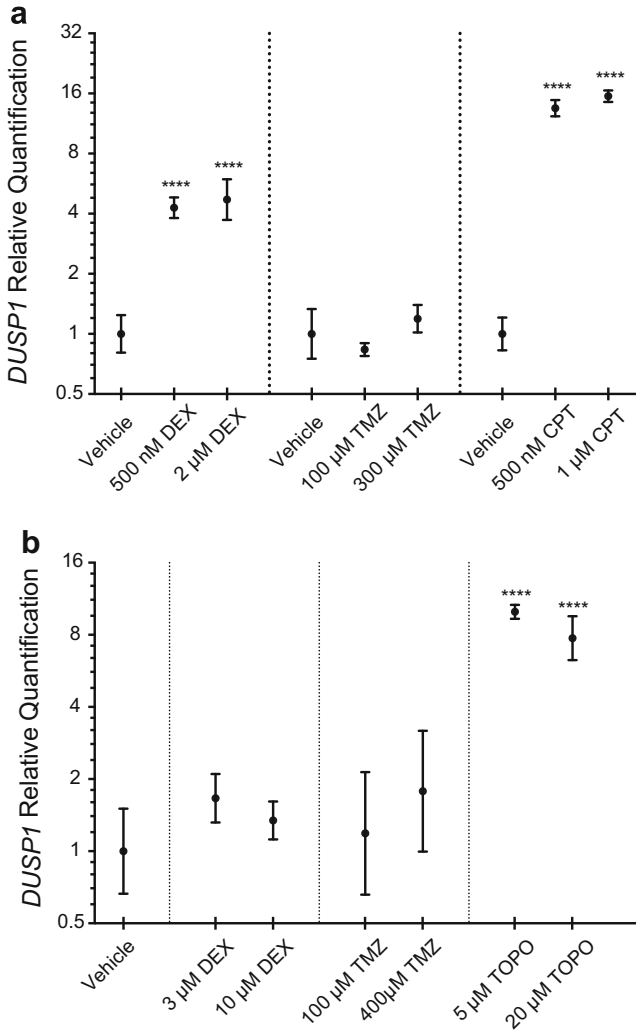

Fig. 6 *DUSP1* regulation by GB chemotherapeutic agents. U251 and U343 GB cell lines **(a)** and GB TSCs **(b)** were treated with the steroid dexamethasone (DEX), or the chemotherapeutics temozolomide (TMZ), camptothecin (CPT), and topotecan (TOPO) for 24 h. Fold-induction responses for *DUSP1* gene expression were determined by qPCR analysis relative to vehicle (DMSO) treated controls and are presented on a log2 scale ($n = 3$ per group). Statistical significance was assessed using one-way ANOVA with Bonferroni correction to account for multiple comparisons (**** = $p < 0.0001$)

Using non-parametric Spearman correlations, results show an inverse relationship between *DUSP1* and each of the TSC markers studied as shown (*ABCG2*: $r = -0.09$, $p = 0.05$; *PROM1*: $r = -0.13$, $p = 0.003$; *L1CAM*: $r = -0.16$, $p = 0.001$; *NANOG*: $r = -0.19$, $p < 0.0001$; *SOX2*: $r = -0.21$, $p < 0.0001$).

To directly assess the dependence of *DUSP1* expression on differentiation, we induced differentiation in TSC cultures and harvested RNA for qRT-PCR. As expected, TSC differentiation resulted in the downregulation of the stem cell marker *SOX2* (5962 A.U. vs. 755 A.U.), and increased expression of mature glial (*GLAST1*; 43 A.U. vs. 135 A.U.) and neuronal (*NEUROD1*; 241 A.U. vs. 454 A.U.) markers measured by

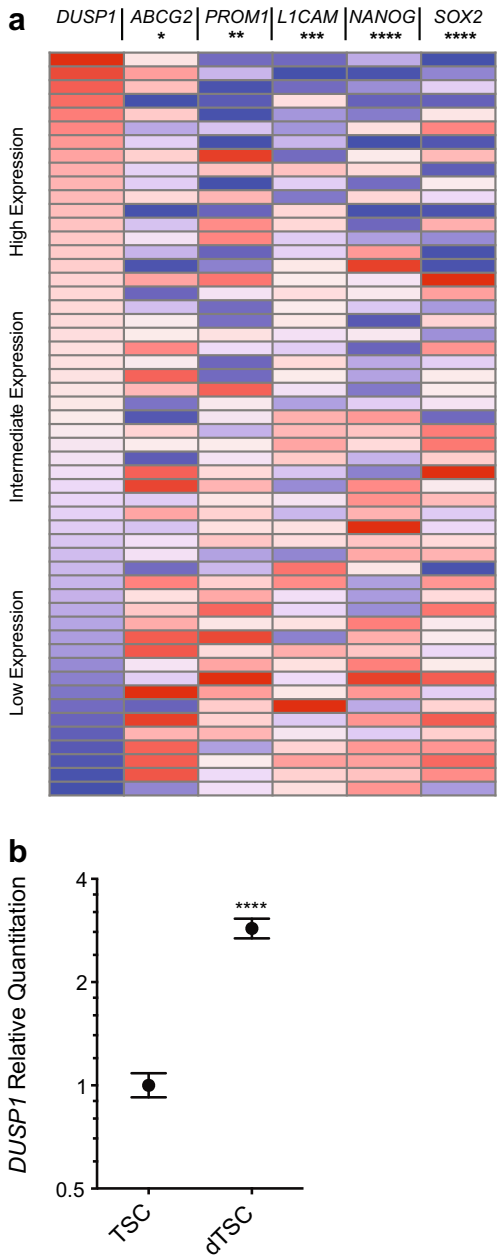

Fig. 7 *DUSP1* expression correlates with markers of GB TSC differentiation. **a** Expression heat maps for *DUSP1* and the differentiation markers *ABCG2*, *PROM1*, *L1CAM*, *NANOG*, and *SOX2* in GB samples from the TCGA microarray dataset (n = 547). Gene expression was normalized to the maximum expression values, sorted from max to min *DUSP1* expression, and stratified into ten sample bins that are displayed as an average gene expression heatmap. Significance testing was performed using two-tailed, non-parametric Spearman correlation of *DUSP1* with the known TSC markers (* = $p < 0.05$, ** = $p < 0.01$, *** = $p < 0.001$, **** = $p < 0.0001$). **b** qPCR analysis of *DUSP1* expression in a patient-derived GB TSC line cultured for three days *in vitro* under conditions of serum-based differentiation. Fold induction of *DUSP1* are plotted against the Log2 scale for differentiated (dTSC) group relative to undifferentiated stem cells (TSCs; n = 3 per group). Significance testing was performed using a t-test (**** = $p < 0.0001$)

FACS (Fig. S1) [28, 29]. TSC differentiation was also associated with a reduction in average cell size measured by forward scatter (70,744 A.U. vs. 36,595 A.U.). Notably, qRT-PCR analysis demonstrated increased *DUSP1* expression with induced TSC differentiation (1.00 [+0.08, −0.08] vs. 2.87 [+0.20, −0.18], $p < 0.0001$; Fig. 7b).

Given the link between *DUSP1* and GB TSC maturity, we next asked whether *DUSP1* expression correlated with TSC populations *in situ*. Using the panel of seventeen GB TSC markers from the Ivy GAP protocol, we first established the location of TSC clusters within GB biopsy specimens relative to the standard histological markers (Fig. 8a). As expected, most TSCs were clustered around regions of necrosis, including the CTpan (18%) and CTpnz (30%). Additional foci were identified around microvascular structures including hyperplastic blood vessels (CThbv: 23%) and regions of microvascular proliferation (CTmvp: 3%). The expression of *DUSP1* in TSC clusters micro-dissected from CTpan and CTpnz structures were not elevated to a significant degree relative to levels observed in TSC clusters found within the cellular tumor region (CT: 64.11±65.27; CTpan: 76.41±35.01; CTpnz: 119.7±114.1; Fig. 8b).

Discussion

The purpose of this work was to establish the expression pattern of the family of human dual specificity phosphatases (*DUSPs*) across primary glioblastoma (GB) samples and to investigate whether the observed changes in one or more *DUSP*s might serve as a therapeutic target for this devastating condition. Employing a combination of *in silico* and *in vitro* approaches, we found that relative to other *DUSPs*, *DUSP1* and *DUSP6* exhibited the highest-level expression in normal CNS tissue specimens as well as across a broad range of human GB tumors. Although we noted significant variability between the DUSPs across the tumor microenvironment of clinical specimens, three transcriptional signatures emerged characterized by transcriptional induction (*DUSP4 & 6*), repression (*DUSP2, 7, 8, & 9*), and a mixed phenotype (*DUSP1, 5, 10, & 16*). And in the case of *DUSP1*, we corroborate these findings *in vitro* demonstrating the stimulatory effect of hypoxia or several chemotherapeutic drugs on *DUSP1* expression. Finally, based on changes observed in our analyses of the IVY Consortium *in situ* data set, we found that *DUSP1* is induced under conditions of TSC differentiation, suggesting that DUSP1 dysregulation may play a role in the maintenance and self-renewal of the stem cell population in GBM tumors.

Our results reveal marked diversity in the basal pattern of *Dusp* expression across cells comprising the adult mammalian CNS. Unlike the rather broad expression exemplified by other *Dusps*, expression of *Dusp4 & 8* was restricted largely to neurons while *Dusp2 was expressed* predominantly by microglia. Conversely, analyses revealed that *DUSP1* and *DUSP6* exhibited broad, high-level expression in both non-

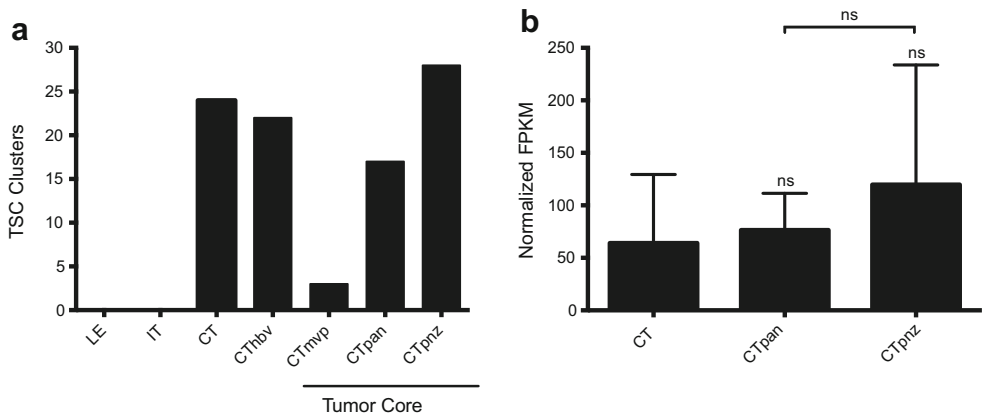

Fig. 8 *DUSP1* expression in perinecrotic regions within GB tumors. **a)** Quantification of TSC clusters identified and microdissected per GB subregion (LE = leading edge, IT = infiltrating tumor, CT = cellular tumor, CThbv = hyperplastic blood vessels, CTmvp = microvascular proliferation, CTpan = pseudopalisading cells around necrosis, CTpnz = perinecrotic zone) in Ivy GAP datasets. **b** *DUSP1* RNA-seq data expressed as normalized fragments per kilobase of transcript per million mapped reads (FPKM) were obtained from the Ivy GAP consortium. TSC clusters identified in GB specimens were segmented into discrete tumor sub-regions including bulk cellular tumor (CT, n = 22), pseudopalisading cells around necrosis (CTpan, n = 16) and the perinecrotic zone (CTpnz, n = 26). Statistical analyses were performed using one-way ANOVA using Bonferroni to correct for multiple comparisons (ns = not significant)

transformed CNS tissue and glioblastoma tumor specimens. This is noteworthy considering the distinct and complementary subcellular localization of *DUSP1* (nuclear) and *DUSP6* (cytoplasmic) and MAPK specificity (JNK, P38, ERK vs. ERK, respectively). While we did not validate *Dusp6* expression under basal or stress-induced conditions, these results suggest that DUSP1 & DUSP6 play a dominant role in regulating MAPK signaling and other emergent properties in GB tumors over those conveyed by the remaining *DUSP* family members.

To explore the transcriptional landscape of *DUSP* expression in glioblastoma and generate hypotheses regarding DUSP function in this context, we also performed *in silico* analyses using datasets from several publically available tumor registries. The tumor-suppressive capacities of various DUSP family members including the cytosolic ERK-specific *DUSP6* and *DUSP9* have been described elsewhere [8]. Similarly, *DUSP4* overexpression inhibits colony formation via effects on proliferation *in vitro* [12]. Although we expected expression to be attenuated through either mutation or epigenetic suppression of the tumor suppressor and transcriptional regulator TP53 [12, 30], *DUSP4* mRNA was in fact induced in the majority of registered REMBRANDT samples. Conversely, multiple ERK-specific members including *DUSP2, 7, & 9* were downregulated in these analyses. Considering how often activating mutations and overexpression of the EGFR receptor are observed in GB tumors, it is interesting to consider the dramatic effects that loss of one or more DUSPs would have on overall ERK1/2 activity. Given its importance in promoting chemotherapeutic resistance in GB through high affinity, inhibitory effects on JNK activity [11], our observation of high-level DUSP6 expression broadly across the tumor microenvironment seems particularly relevant. And, while other DUSP family members may well influence glioma biology, based on their broad and high-level expression, our data argue that manipulation of both *DUSP1* and *DUSP6* would likely confer the greatest therapeutic benefit in GB.

We also studied inducible *DUSP1* transcription *in vitro* using both GB cell lines and patient-derived TSCs exposed to hypoxia [15], dexamethasone [16], and DNA damaging agents [31, 32]. While our results confirmed hypoxia and dexamethasone inducibility, we identified that while treatment with the topoisomerase I inhibitors camptothecin (CPT) and topotecan (TOPO) activated *DUSP1* transcription, the standard of care DNA alkylating agent temozolomide (TMZ) did not. Why might this be the case? Where CPT and TOPO specifically inhibit the topoisomerase I DNA damage response leaving single and double strand breaks in the phosphodiester backbone, DNA alkylating agents like TMZ rely on defects in the DNA damage response for maximum therapeutic efficacy. TMZ-induced O6 guanine alkylation is reversed under conditions where the O6-methylguanine-DNA-methyltransferase (MGMT) is maximally expressed, which in turn prevents subsequent DNA mismatch repair-mediated cell death [33]. However, methylation-induced repression of the MGMT promoter is present in 40% of GB cases and provides an opportunity for TMZ to extend patient survival by 6.4-months [34, 35]. The lack of a *DUSP1* response to TMZ *in vitro* may reflect insufficient levels of DNA damage induced by this particular chemotherapeutic agent.

The hypoxic core in GB tumors is enriched in cells with stem-like properties including multipotency and the capacity for self-renewal. These cells are also resistant to chemotherapeutic toxicity and likely contribute to secondary tumor recurrence [21]. Reports regarding the relationship between DUSP

regulation and the state of cellular differentiation are mixed [22–24]. For example, while *DUSP1* is induced in differentiating adipocytes [36], increased ERK1/2 phosphorylation (indicative of low DUSP activity) enhances both the metabolism [37] and differentiation of neural progenitor cells [38]. In other studies, *Dusp1*$^{-/-}$ mice exhibit metabolic amplification in response to overactive MAPK signaling [39].

We were particularly interested to understand the potential relationship between *DUSP1* regulation and the tumor stem cell niche. First, we found that DUSP1 expression increased in differentiated cultures of patient-derived TCS confirmed using standard markers. Of note, analysis of *DUSP1* expression within TSC-rich regions of the tumor microenvironment using the IVY Consortium data set revealed no significant changes between cellular tumor (CT), hypoxic pan necrosis (CTpan), and perinecrotic (CTpnz) regions. Given our observation that average *DUSP1* expression was induced within the core region of GBM tumors (Fig. 4), failure to induce *DUSP1* within the stem cell niche could reflect either the loss of one or more factors required for transcriptional activation or possibly the persistent expression of a transcriptional repressor. Like *DUSP4*, *DUSP1* is both a transcriptional target of TP53 [31] and an important effector in P53-dependent cell cycle regulation and apoptosis [31, 32]. Notably, loss of *dusp1* expression in *Tp53*$^{-/-}$ mice results in the upregulation of several genes that promote NSC survival and proliferation [40]. This observation is particularly relevant in the transformed tumor stem cell background since 87% of GB cases harbor aberrations in *TP53* activity leading to enhanced TSC self-renewal [41].

While our use of several well characterized cancer genomics datasets was a fruitful platform for generating novel hypotheses regarding the role of DUSP regulation in glioblastoma, the limitations inherent to this approach should be acknowledged. While we have validated the regulation of four *DUSP* family members in homogenized bulk tumors, further study will be required to determine whether the data from our *in silico* analyses accurately reflect the pattern of DUSP expression within discrete cells of the mature cortex and regions of the tumor microenvironment. Additionally, our focus on transcriptional responses overlooks the complex interactions across the network of MAPK-DUSP since shifts in DUSP1 protein stability and sub-cellular localization impinge on a wide array of MAPK-dependent processes. For example, growth factor stimulation of the MAPKs by ERK1/2 and p38 leads to increased production of *DUSP1* mRNA [42]. ERK1/2-dependent phosphorylation of DUSP1 protein at $S^{359/364}$ also enhances its turnover via ubiquitin-dependent degradation, a process that is reversed under conditions in which the ubiquitin-proteasome complex is inhibited [43]. However, our ability to study DUSP1 at the protein level is impeded by the lack of reliable DUSP1 antisera capable of distinguishing total from modified forms DUSP1 from other members of the DUSP family (data not shown).

In conclusion, we present results from a systematic analysis of *DUSP* family mRNA expression in glioblastoma multiforme. While our initial interrogation of *DUSP* expression revealed uniform trends for several factors, signals for others including DUSP1 were mixed and otherwise obscured by signal averaging in homogenized bulk tumor specimens. Using a complementary *in silico* approach, we found DUSP1 exhibited marked heterogeneity in expression across the tumor microenvironment. Subsequent analyses performed *in vitro* identified several potential mediators of *DUSP1* inducibility including hypoxic stress as well as exposure several clinically relevant chemotherapeutic agents. We also demonstrate that *DUSP1*, along with other traditional markers, is induced in differentiated, patient-derived tumor stem cells. Analyses of cancer stem cell RNA-Seq data derived from primary glial tumors suggest a failure to induce*DUSP1* expression in regions of significant intratumoral stress. And although not directly tested here, our findings argue that approaches geared towards reactivating *DUSP1* expression *in situ* may render this otherwise refractory cell population sensitive to therapeutic intervention.

Acknowledgments This project was funded by awards from the National Institutes of Health to Marc W. Halterman (R01-NS076617) and Bradley N. Mills (F31-CA180358).

References

1. Rong Y et al (2006) 'Pseudopalisading' necrosis in glioblastoma: a familiar morphologic feature that links vascular pathology, hypoxia, and angiogenesis. J Neuropathol Exp Neurol 65(6):529–539
2. Persano L et al (2011) The three-layer concentric model of glioblastoma: cancer stem cells, microenvironmental regulation, and therapeutic implications. Sci World J 11:1829–1841
3. Vartanian A et al (2014) GBM's multifaceted landscape: highlighting regional and microenvironmental heterogeneity. Neuro-Oncology 16(9):1167–1175
4. Li Z et al (2009) Hypoxia-inducible factors regulate tumorigenic capacity of glioma stem cells. Cancer Cell 15(6):501–513
5. Li Z et al. (2009) Hypoxia-inducible factors regulate tumorigenic capacity of glioma stem cells. In: Cancer Cell. Elsevier Ltd. p 501–513
6. Vitucci M et al (2013) Cooperativity between MAPK and PI3K signaling activation is required for glioblastoma pathogenesis. Neuro-Oncology 15(10):1317–1329
7. Raman M, Chen W, Cobb MH (2007) Differential regulation and properties of MAPKs. Oncogene 26(22):3100–3112
8. Boutros T, Chevet E, Metrakos P (2008) Mitogen-activated protein (MAP) kinase/MAP kinase phosphatase regulation: roles in cell growth, death, and cancer. Pharmacol Rev 60(3):261–310
9. De Witt Hamer PC (2010) Small molecule kinase inhibitors in glioblastoma: a systematic review of clinical studies. Neuro-Oncology 12(3):304–316
10. Yu H et al (2012) Constitutive expression of MAP kinase phosphatase-1 confers multi-drug resistance in human glioblastoma cells. Cancer Res Treat 44(3):195–201

11. Messina S et al (2011) Dual-specificity phosphatase DUSP6 has tumor-promoting properties in human glioblastomas. Oncogene 30(35):3813–3820
12. Waha A et al (2010) Epigenetic downregulation of mitogen-activated protein kinase phosphatase MKP-2 relieves its growth suppressive activity in glioma cells. Cancer Res 70(4):1689–1699
13. Wayne J et al (2006) ERK regulation upon contact inhibition in fibroblasts. Mol Cell Biochem 286(1–2):181–189
14. Sakaue H et al (2004) Role of MAPK phosphatase-1 (MKP-1) in adipocyte differentiation. J Biol Chem 279(38):39951–39957
15. Laderoute KR et al (1999) Mitogen-activated protein kinase phosphatase-1 (MKP-1) expression is induced by low oxygen conditions found in solid tumor microenvironments. A candidate MKP for the inactivation of hypoxia-inducible stress-activated protein kinase/c-Jun N-terminal protein kinase activity. J Biol Chem 274(18):12890–12897
16. Lin YM et al (2008) Dexamethasone reduced invasiveness of human malignant glioblastoma cells through a MAPK phosphatase-1 (MKP-1) dependent mechanism. Eur J Pharmacol 593(1–3):1–9
17. Scarpace L et al. (2015) Data from REMBRANDT. The Cancer Imaging Archive. Available from: https://doi.org/10.7937/K9/TCIA.2015.588OZUZB
18. Zhang Y et al (2014) An RNA-sequencing transcriptome and splicing database of glia, neurons, and vascular cells of the cerebral cortex. J Neurosci 34(36):11929–11947
19. Ivy (2015) Ivy Glioblastoma Atlas Project Available from: http://glioblastoma.alleninstitute.org/rnaseq
20. NCI (2015) The cancer genome atlas; Available from: https://www.cancer.gov/
21. Galli R et al (2004) Isolation and characterization of tumorigenic, stem-like neural precursors from human glioblastoma. Cancer Res 64(19):7011–7021
22. Inuzuka H et al (1999) Differential regulation of immediate early gene expression in preadipocyte cells through multiple signaling pathways. Biochem Biophys Res Commun 265(3):664–668
23. Sahu M, Mallick B (2016) An integrative approach predicted co-expression sub-networks regulating properties of stem cells and differentiation. Comput Biol Chem 64:250–262
24. Boulding T et al (2016) Differential roles for DUSP family members in epithelial-to-mesenchymal transition and cancer stem cell regulation in breast cancer. PLoS One 11(2):e0148065
25. Bleau AM, Huse JT, Holland EC (2009) The ABCG2 resistance network of glioblastoma. Cell Cycle 8(18):2936–2944
26. Hjelmeland AB et al (2011) Twisted tango: brain tumor neurovascular interactions. Nat Neurosci 14(11):1375–1381
27. Bradshaw A et al (2016) Cancer stem cell hierarchy in glioblastoma Multiforme. Front Surg 3:21
28. Martinez-Lozada Z et al (2014) Activation of sodium-dependent glutamate transporters regulates the morphological aspects of oligodendrocyte maturation via signaling through calcium/calmodulin-dependent kinase IIbeta's actin-binding/−stabilizing domain. Glia 62(9):1543–1558
29. Roybon L et al (2009) Neurogenin2 directs granule neuroblast production and amplification while NeuroD1 specifies neuronal fate during hippocampal neurogenesis. PLoS One 4(3):e4779
30. Shen WH et al (2006) Mitogen-activated protein kinase phosphatase 2: a novel transcription target of p53 in apoptosis. Cancer Res 66(12):6033–6039
31. Li M et al (2003) The phosphatase MKP1 is a transcriptional target of p53 involved in cell cycle regulation. J Biol Chem 278(42):41059–41068
32. Liu YX et al (2008) DUSP1 is controlled by p53 during the cellular response to oxidative stress. Mol Cancer Res 6(4):624–633
33. Lord CJ, Ashworth A (2012) The DNA damage response and cancer therapy. Nature 481(7381):287–294
34. Esteller M et al (2000) Inactivation of the DNA-repair gene MGMT and the clinical response of gliomas to alkylating agents. N Engl J Med 343(19):1350–1354
35. Hegi ME et al (2005) MGMT gene silencing and benefit from temozolomide in glioblastoma. N Engl J Med 352(10):997–1003
36. Ferguson BS et al (2016) Mitogen-dependent regulation of DUSP1 governs ERK and p38 signaling during early 3T3-L1 adipocyte differentiation. J Cell Physiol 231(7):1562–1574
37. Kim DY, Rhee I, Paik J (2014) Metabolic circuits in neural stem cells. Cell Mol Life Sci 71(21):4221–4241
38. Li Z, Theus MH, Wei L (2006) Role of ERK 1/2 signaling in neuronal differentiation of cultured embryonic stem cells. Develop Growth Differ 48(8):513–523
39. Wu JJ et al (2006) Mice lacking MAP kinase phosphatase-1 have enhanced MAP kinase activity and resistance to diet-induced obesity. Cell Metab 4(1):61–73
40. Meletis K et al (2006) p53 suppresses the self-renewal of adult neural stem cells. Development 133(2):363–369
41. Cancer Genome Atlas Research, N (2008) *Comprehensive genomic characterization defines human glioblastoma genes and core pathways*. Nature 455(7216):1061–1068
42. Li J et al (2001) Transcriptional induction of MKP-1 in response to stress is associated with histone H3 phosphorylation-acetylation. Mol Cell Biol 21(23):8213–8224
43. Brondello J (1999) Reduced MAP kinase phosphatase-1 degradation after p42/p44MAPK-dependent phosphorylation. Science 286(5449):2514–2517